Fuel 352 (2023) 129076

Contents lists available at ScienceDirect

Fuel

journal homepage: www.elsevier.com/locate/fuel

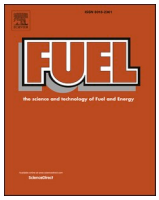

Full Length Article

Assessment of injector-flow characteristics of additised and renewable diesel blends through high-speed imaging

Onur Baran [a,b,*], Ioannis K. Karathanassis [a,b], Phoevos Koukouvinis [a,b], Joonsik Hwang [c], Lyle M. Pickett [b], David Spivey [d], Manolis Gavaises [a]

[a] School of Science & Technology, City, University of London, Northampton Square, EC1V 0HB London, UK
[b] Combustion Research Facility, Sandia National Laboratories, 7011 East Avenue, Livermore, CA 94550, USA
[c] Centre for Advanced Vehicular Systems (CAVS), Department of Mechanical Engineering, Mississippi State University, Starkville, MS 39762, USA
[d] Lubrizol Limited, Nether Lane, Hazelwood, Belper, Derbyshire DE56 4AN, UK

A B S T R A C T

The influence of additives inducing viscoelasticity in diesel fuel, on the in-nozzle cavitation evolution and the expelled spray morphology has been quantified by high-speed, diffused back-light and schlieren imaging applied to two single-hole true-scale transparent injectors of straight and tapered orifice layouts (so-called Spray C and D of the engine Combustion Network), as well as a five-hole configuration (Spray M). More specifically, the in-nozzle cavitating flow and its effect on near-nozzle spray formation of a non-Newtonian diesel fuel sample treated with Quaternary Ammonium Salt (QAS) additives and exhibiting viscoelastic effects, as well as biodiesel (FAME), are compared against conventional diesel fuel for the first time. The operating conditions corresponded to injection and ambient pressures in the range of 500–900 bar and 1–20 bar, respectively. It was found that viscoelasticity has an overall suppressing effect on wall-attached, or so-called geometrical, cavitation. Furthermore, the investigation revealed that the action of viscoelastic additives has the capability to enhance the magnitude of well-established longitudinal vortices, with the subsequent after-effect of leading to increased cone angles of the expelled spray. On the contrary, it tends to suppress turbulence-induced transient instabilities in a manner similar to turbulence suppression.

1. Introduction

While electrification has the potential to transform the powertrain in many vehicles, the majority of medium and heavy-duty vehicles currently rely on internal-combustion engines for propulsion, and this trend is expected to persist in the foreseeable future, particularly for long-range and off-road applications. It is forecasted that by 2040, approximately one-third of medium and heavy-duty truck sales will be electric worldwide [1]. Meanwhile, upcoming regulations necessitate the reduction of tailpipe soot, NOx, and CO_2 emissions. For instance, the Euro VII standard dictates a decrease in NOx emissions from automobiles by 35 % and by 56 % in buses and lorries compared to Euro VI [2]. Therefore, the pursuit of increasing the fuel and environmental efficiency of modern diesel engines remains timely. The pathway for accomplishing these objectives is inherently linked with the enhancement of combustion quality, for instance, through the optimisation of the fuel atomisation behaviour and subsequent mixing with air.

As the fuel injection system is a critical part of the diesel engine, it directly affects combustion performance and exhaust emission rates [3]. This reveals that the flow processes occurring within the injector's complicated flow path have a vital influence on fuel delivery and engine performance. Modern diesel injectors have orifice diameters of the order of 150 μm and operate at injection pressures higher than 2500 bar. Such extreme operating conditions in combination with the geometrical layout of the nozzle holes that cause a flow restriction, cause cavitation to form within the injector nozzles. Cavitation formation within diesel injectors has been extensively investigated with the incorporation of either real-size or enlarged transparent tips replicating the sac and injector-hole layouts of the device. Visualisation of in-nozzle cavitation is challenging owing to the highly turbulent nature of the flow and the very small length and time scales of process evolution. Imaging with diffuse-light techniques [4,5], i.e., either Mie scattering or backlight imaging has been employed on numerous occasions to provide insight into the morphological characteristics of vapour cavities emerging in high-pressure diesel injectors and correlate them with the atomisation and dynamics of the fuel spray delivered by the devices [6,7]. Some early and representative studies expanding over a wide range of conditions and nozzle configurations include [8–10]. More specifically, Desantes et al. [8] tested single-hole injectors of varying hole diameters operating at different pressure differences to illustrate the influence of

* Corresponding author at: School of Science & Technology, City, University of London, Northampton Square, EC1V 0HB London, UK.
E-mail address: onur.baran@city.ac.uk (O. Baran).

https://doi.org/10.1016/j.fuel.2023.129076
Received 4 April 2023; Received in revised form 6 June 2023; Accepted 21 June 2023
Available online 1 July 2023

geometry and operating conditions on cavitation development. Mitroglou et al. [9] obtained a multitude of in-nozzle flow, high-speed images from identical diesel injectors that enabled the production of ensemble-average images indicating the probability of cavitation appearance at a specific location within the injector nozzle. In a subsequent study, Mitroglou et al. [10] visualised the two-phase flow in a Valve Covered Orifice (VCO) injector and demonstrated the correlation of different cavitation regimes with the near-nozzle spray morphology.

The formation and dynamic evolution of vaporous structures within the injector affect its discharge coefficient, the dynamics and composition of the expelled spray [11–13] and pose a threat to the injector rigidity [14–16]. Transparent tips have been usually made from acrylic or even quartz which, are capable of withstanding extreme pressures up to 2000 bar [17,18]. Recently, advancements in X-ray technology have also made it possible to investigate real-size steel nozzles [19,20].

From those indicative studies, many of which come from the authors' group, two primary cavitation regimes have been identified within injector nozzles, namely sheet/cloud cavitation and vortex or string cavitation [3]. The former regime arises in regions adjacent to solid boundaries due to local flow separation, whereas the latter is probable to emerge in the nozzle core. The different cavitation regimes emanating due to flow acceleration, as well as separation and coherent vortical motion [21] have been elucidated and correlated to spray morphology [22] and erosion patterns [23]. These phenomena are also relevant to the present work, as they have been conducted only with standard diesel and thus, serve as a reference for comparison with the new fuels tested and reported as part of the present investigation. Moreover, relevant to the present work are also the recent studies of Karathanassis et al. [7] and Manin et al. [18] who applied high-speed stereoscopic microscopy to investigate the two-phase flow field in the so-called transparent nozzle Spray D, utilised by the Engine Combustion Network (ECN). In [7] the underlying compressible flow dynamics effects during the needle valve opening and closing allowed elucidation of the gas exchange process taking place after the end of injection with ingestion of ambient gas into the nozzle's sac volume; relevant simulations also have been reported recently in [7,24]. This gas exchange was reported to influence the injection start of the subsequent event, as gas being injected concurrently with the liquid fuel resulted in improved atomisation but also in irregular-shaped fuel structures depositing on the external surface of the injector nozzle tip.

The macroscopic cavitation topology has been demonstrated to be similar between enlarged replicas and real-size nozzles [20], although bubble residence and collapse times are different [25]. Owing to the rapid advancement of micro-fabrication and imaging technologies in the last decade, real-size injectors with transparent tips have been materialised for use in cavitation visualisations [22,26,27]. Transparent tips are made from acrylic, have high optical transparency and are capable of withstanding extreme pressures up to 1000 bar [18].

Modern fuel injection systems incorporate multiple nozzle holes, offering increased spray control and overall atomisation quality [28,29]. Yet, experimental investigations of flow and cavitation inside multi-hole transparent injectors are scarce in the literature owing to fabrication and structural limitations associated with the transparent tips. Furthermore, multiple injector orifices are commonly arranged symmetrically around the sac, hindering visual access to the complex internal flow path [30]. Yasutomi et al. [31] investigated multi-hole and single-hole transparent nozzles using high-speed, long-distance microscopy. Experimental results showed that the axial-hole optical tip hardly displayed any bulk cavitation during the needle closure event, unlike the multi-hole layout for which extensive cavitation formed followed by gas exchange with the ambient. Huang et al. [29] examined the impact of injector hole number on the spray dynamics by X-ray phase-contrast imaging. They found that as the number of holes increased, the near-nozzle spray dynamics varied in a non-monotonical manner. Additionally, the sprays became highly dispersed and fluctuated for the lower hole numbers, along with a rapid decrease in their velocity. Mitroglou et al. [9] visualised real-size, multi-hole nozzles to elucidate shot-to-shot variation in the internal nozzle flow and link the presence of string cavitation to spray angle fluctuations.

All of the aforementioned in-nozzle flow studies have been performed using standard diesel fuel. Parallel to those, numerous studies have investigated the influence of fuel thermodynamics and transport properties on cavitation development and spray dynamics. Fuel properties are generally known to affect spray atomisation [32,33]. Fuel properties such as viscosity and density have been found to significantly change as a function of injection pressure and liquid temperature, as reported by the relevant experimental and computational studies reported recently in [34–41] which reported variations for pressures as high as 3000 bar and temperatures up to 560 K. The influence of those on the cavitation of multi-component fuel surrogates has also been investigated in [42]; significant variations of the cavitation structures and vapour composition have been reported, with pressure increase to values up to 4500 bar. In addition, fuel composition and the mixing of fuels can be additional influential factors. For example, Mo et al. [43] investigated the atomisation quality of pure soybean biodiesel along with a sample blended with 20 % butanol. It was found that the addition of alcohol facilitated spray primary break-up due to its lower viscosity and surface tension.

In addition to those, deposit formation in the nozzle holes hampers the operation of fuel injectors, as it modifies the internal flow field and can cause a deterioration of fuel-delivery performance [44]. Doping the fuel with viscoelasticity-inducing agents, such as some Quaternary Ammonium Salts (QAS), constitutes a well-established method to prevent deposit formation and clean the injector holes. From a broader perspective, the influence of additives on diesel combustion has been thoroughly studied over the years. Due to their proprietary nature and relatively complex chemical structures, additives and mechanisms by which they affect injector flow, spray, and soot formation have not been well studied. Deposit control additives are one of the most important components in a Diesel additive package and are used for suppressing deposit formation and thus, reducing soot formation during long-term operation. Their mechanisms include keeping new injectors clean by generating a protective film on metal surfaces and by preventing agglomeration of deposit precursors, as well as cleaning up fouled injectors by deposit removal and dispersion [45]. Detergents patented for use in diesel applications include Polyisobutylene Succinimides [46], alkyl quaternary ammonium salts based on Polyisobutylene as well as polymeric quaternary ammonium salts [47]. Other additives referred to as soot reducers as well as ignition improvers (cetane improvers) have also long been studied but are out of the scope of the present work. In brief, such additives are able to suppress soot formation in diesel engines and reduce ignition delay, respectively. Compared to traditional metallic soot-reducing additives [48], ashless soot reducers have recently been investigated [49]; Tripropylene Glycol Methyl Ether has been proposed as a viable soot-reducing additive due to a higher efficacy compared to other oxygenates [50,51]. 2-Ethyl Hexyl Nitrate and di-Tert Butyl Peroxide are two of the most widely used cetane improvers.

Nevertheless, relevant studies do not report in detail the influence of additives on nozzle flow. In this area, only a handful of recent studies are available. The work of Barbour et al. [52] constituted an initial experimental study where increase of the injector discharge coefficient was observed for QAS-treated fuel samples. This initial finding led to follow-up studies from the authors' group [53,54], which have focused on the elucidation of the flow processes leading to the measured increase of nozzle flow rate for the same pressure drop [48,49]. Advanced diagnostics including high flux X-ray phase contrast imaging (XPCI) has been employed together with numerical simulations considering the effects of viscoelasticity in cavitating flows [53–56]. These investigations suggested that tested QAS additives when diluted in hydrocarbon fuels, result in micelles forming and bestowing the mixture a viscoelastic nature. The flexible structures interact with coherent vortical motion both in the micro- and the macroscale. The overall

action, perceived macroscopically as viscoelasticity, tends to suppress attached cavitation formed due to cross-flow vortices, while on the contrary, enhances vortical cavitation emanating from longitudinal vortices. These conclusions were established in single-orifice injector replicas promoting a stronger and steadier recirculation pattern compared to multi-hole nozzles. A recent study also from the authors' group on real-size gasoline injectors under realistic operating conditions [57] revealed that viscoelasticity tends to suppress turbulence-induced instabilities, which could potentially give rise to highly transient, vortical cavities with lifetimes of a few tens of microseconds; this time scale although it corresponds to ~ 1/100 of a typical injection duration event, is equivalent to the fuel residence time inside the fuel injector, and thus, long enough to influence the nozzle flow.

All previous studies examining the effect of viscoelasticity on diesel fuels refer only to internal nozzle flow development. To the authors' best knowledge, no prior study has been reported on the quantification of viscoelastic additives on near-nozzle spray angle, while linking them with the internal nozzle flow. Therefore, new results obtained at the combustion facility of SNL utilising the standardised ECN nozzles and operating conditions are reported here for the first time. This has allowed direct comparison of the tested additised samples against prior tests obtained with conventional diesel as well as biodiesel samples. Moreover, different optical injector layouts, namely Spray C, D and M of ECN have been utilised in order to pinpoint differences regarding in-nozzle cavitation and spray morphology. The significance and long-term impact of this work are relevant to the development of sustainable renewable fuels, which appears as a viable and attractive alternative for the decarbonisation of heavy-duty vehicles and earth-moving machines, where current electrification technologies do not seem mature enough to be readily incorporated. As such new fuels exhibit in general compromised rheological properties compared to the standard diesel fuel, utilisation of additives that can alter and improve nozzle flow and atomisation, while they can be standardised and become an integral part of the fuel package, are considered essential for the broader utilisation of such future fuel alternative options.

The rest of the paper is organised as follows: the experimental setup is described, together with the operating conditions, the visualisation setup and the employed measurement techniques. Then the obtained results are presented in a comparative manner between the tested fuel samples. Finally, the most important conclusions are summarised at the end.

2. Experimental campaign

Three types of diesel fuel were assessed in a comparative manner in this investigation: (i) a standard commercial diesel fuel (base diesel), (ii) a base sample treated with Quaternary Ammonium Salts (QAS) at a concentration of 1000 mg/kg (additised diesel), which bestow the fluid non-Newtonian, viscoelastic rheology and (iii) a Fatty Acid Methyl Ester (FAME) biodiesel. As already mentioned, the suspension of QAS additives in diesel fuel has been demonstrated to lead to the formation of flexible micelles, which interact with vortical structures at different length scales and eventually influence the cavitation topology [53]. Fuel samples were selected to highlight differences between 'engineered' fuel blends, commercial blends and renewable counterparts. Samples were tested at room temperature, and their relevant bulk properties are summarised in Table 1. Prior measurements [54] have verified that the addition of QAS additives at such concentrations does not affect the thermodynamic and transport properties of the base blend.

Table 1
Nominal fuel properties at 1 bar and 27 °C of the diesel samples utilised in the present investigation [58,59].

Fuel	Base diesel	Additised diesel	FAME
ρ_f [kg/m^3]	830	830	880
ν_f [mm^2/s]	2.6	2.6	3.5
p_{sat} [•10^3 Pa]	17,200	17,200	40,000

2.1. Pressure chamber and fuel-injection system

Experiments were carried out in the sealed cubical pressure vessel depicted in Fig. 1a. Details on the chamber dimensions and structural components have been given in previous investigations [7,31]. In brief, the four sides of the vessel are covered with fused-silica windows enabling simultaneous visualisation with the use of different optical techniques. The pressure inside the vessel is regulated by nitrogen injections through four ports located at the top of the vessel. The fuel-gas mixture after the injection is vented through the exhaust located at the bottom of the vessel. The injection and ambient pressures are recorded by pressure transducers located at the fuel line and the exhaust line, respectively. Fuel is pressurised to a prescribed injection pressure with the use of a syringe pump.

Two different injector geometries standardised by Engine Combustion Network (ECN) [60] were employed for the conducted experiments. Namely, transparent counterparts of the so-called Spray C [61] and Spray D [62] single-hole injectors have been fabricated. Although the two layouts are quite similar in overall dimensions, Spray D is a tapered orifice and, hence, the extent of arising cavitation is expected to be moderate compared to the straight Spray C orifice. An additional five-hole optical injector, shown in Fig. 1b, referred to as Spray M from now on, has been included in the investigation to take into account three-dimensional instabilities occurring in the sac region due to hole-to-hole flow interactions. As also illustrated in the section view of Fig. 1a, acrylic tips were mechanically clamped in between the metallic body of a modified injector, having its tip severed and ground flat and a supporting pedestal holding the tip in place. The pedestal layout is machined in a way to facilitate imaging of the injector near the field. For the single-hole injectors, a metallic pedestal was utilised as described in [7]; however, an acrylic pedestal of more complex geometry was employed in the Spray M investigation. The spray M pedestal realises two draining ducts, annotated in Fig. 1b, in alignment with injector holes to facilitate unobscured optical access to the 'nozzle of interest', as is clarified by the raw images presented in the following section.

2.2. Optical setup

The optical set-up implemented and depicted in Fig. 2 allowed the concurrent application of Diffuse Backlight Illumination (DBI) and schlieren imaging in orthogonal orientation. Two pulsating LEDs, blue (455 ± 22 nm) for DBI and red (620 ± 22 nm) for schlieren, respectively, provided illumination. Complete details of the structural components of the dual-imaging system can be found in [7]. The schlieren set-up sensitivity was properly calibrated to be able to capture liquid density gradients within the nozzle induced by the presence of coherent vortical motion, as discussed in detail in previous work [7]. Longitudinal vortices arising within the injector hole were captured as streak-like refractive index gradients by the schlieren system. Besides, raw schlieren images were utilised to measure the spray-cone angle since they offered a higher contrast in the spray periphery compared to the DBI images.

High-speed images were recorded at 100,000 fps simultaneously by two different CMOS cameras, Photron SA-X2 and Phantom v2512, fitted with long-distance microscopes and triggered concurrently by the injector-driver. The dimensions of the active window were 640 × 176 and 768 × 272 pixels for DBI and schlieren systems, respectively; the corresponding spatial resolutions were 3.90 μm/pixel and 3.24 μm/pixel, respectively.

2.3. Image acquisition and post-processing

A number of post-processing techniques were applied to extract

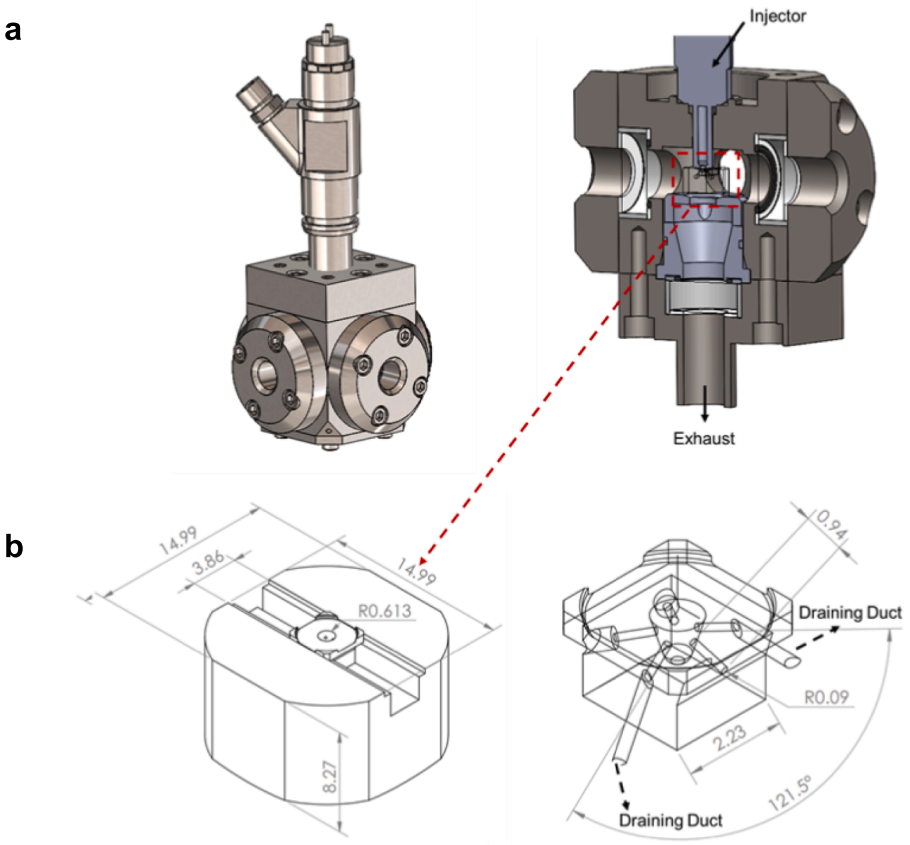

Fig. 1. (a) Overall and section views of the spray chamber employed in the experiments. (b) CAD assembly of the Spray-M test piece with the dedicated acrylic pedestal. All dimensions are in mm.

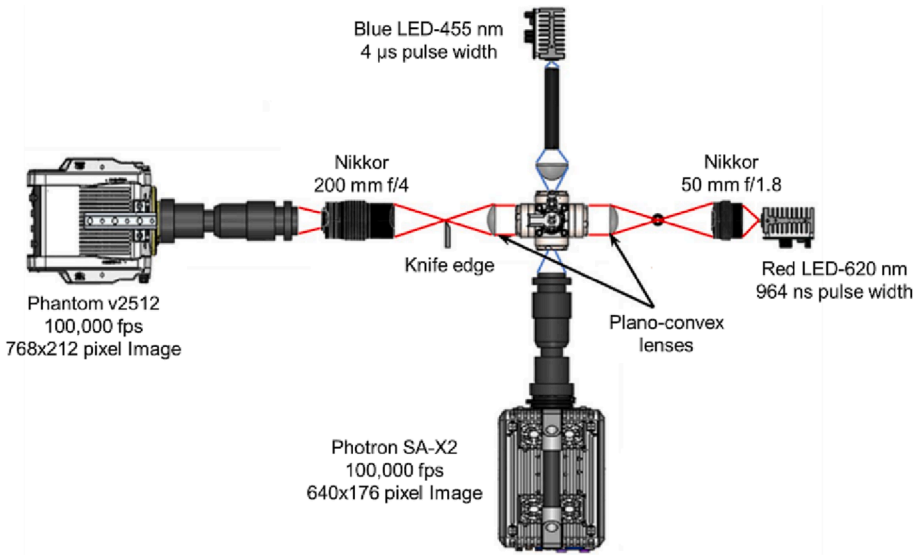

Fig. 2. Schematic of the optical layout for the DBI (red LED) and schlieren (blue LED) imaging systems (reproduced from [7]). (For interpretation of the references to colour in this figure legend, the reader is referred to the web version of this article.)

quantitative data regarding the extent and dynamics of in-nozzle vorticity and cavitation, as well as the temporal variation of the spray cone angle from the high-speed images. The post-processing steps realised through an in-house code for the derivation of the projected area of either vapour cavities or vortices within the injector nozzle are analysed in detail in our previous publication [7]; thus, they are not repeated here in detail. In summary, the region of interest was initially cropped and masked in the raw images, and a background image of stagnant liquid within the injector was subtracted. Based on proper thresholding, black and white images were produced with white pixels corresponding to regions of refractive index gradients, i.e., cavitation or vorticity. Similarly, the region of interest was cropped and binarised on proper thresholding for the spray cone angle calculation. Edges of the binarised image were detected employing the Canny edge detection algorithm.

Denoising of the detected edges was applied to avoid rogue droplets' effect on the measurement. Finally, the centroids of the two edges of the spray were identified, and the spray cone angle was calculated using their positions.

In order to distinguish vortical cavitation from geometric cavitation in the case of the Spray M injector, a bespoke algorithm was developed to record the eccentricity and location of the vaporous structures arising at each frame. The extent of in-nozzle cavitation was quantified using the binarisation method employed in the single-orifice configurations as well (Fig. 3a). Vortical cavitation specifically was identified with the application of suitable thresholds for both the eccentricity and the location of the binarised structure in the nozzle. For instance, cavities in Fig. 3a are classified as vortical cavitation since they exceed the established threshold for eccentricity. The usefulness of the two identification criteria becomes apparent, especially in the entrance region, as illustrated in Fig. 3b. Although the values of eccentricity for the two detected structures are similar, the one indicated by the blue circle is classified as geometric cavitation, while the one in the red circle is considered vortical cavitation owing to their relative location within the orifice.

3. Results and discussion

The experiments conducted in the present investigation are outlined in Table 2. It should be clarified that the injection pressure for the Spray D and Spray M layouts was limited, after preliminary testing, to 900 and 500 bar, respectively to allow for testing of at least four injection events per fuel and ambient condition without rupturing the acrylic piece. Specifically referring to the Spray M layout, the pressure had to be limited to a lower value, as the complex geometry machined out of the acrylic part rendered the piece less rigid than spray D. However, the injection pressure for the Spray C injector was designated by visualisation limitations, since for pressures higher than 700 bar, the injector hole was completely opaque throughout the injection event.

3.1. Single-hole injectors

The results presented in this section refer to the axial-orifice Spray C and Spray D injectors. Indicative sequences of raw images obtained in the single-orifice, Spray C and D, injectors during the campaign are illustrated in Fig. 4. The sequences of Fig. 4a referring to the straight Spray C highlight that the entire injector hole is occupied by vapour, rendering it almost entirely opaque. The video of the injection event provided as Supplementary material (SV_C), however, hints that cavitation forms a vapour sheet adjacent to the hole periphery, while transient features manifest in the orifice core. On the contrary, the tapered

Table 2
Matrix of conducted test cases. The Reynolds number was calculated using the orifice diameter d_o, as a characteristic length scale.

Injector layout	Spray C	Spray D	Spray M
Injection pressure [10^5 Pa]	700	900	500
Ambient gas	N_2		
Ambient temperature [K]	293		
Ambient pressure [10^5 Pa]	1–5–20 5–20 1–5–20		
Ambient density [kg/m^3]	1.15–5.76–23.09		
Re $\left(=\frac{u \bullet d_o}{\nu_f}\right)$	15,370 (700/5 bar) 17,460 (900/5 bar) 12800 (500/5 bar)		
CN $\left(=\frac{p_{inj}-p_{back}}{p_{back}-p_{sat}}\right)$	143–34 (5–20 bar) 185–44 (5–20 bar) 102–24 (5–20 bar)		

layout of Spray D leads to milder cavitation with the majority of the nozzle occupied by pure liquid, as shown in Fig. 4b. Regions of cavitation can be discerned in the nozzle throat and close to the injector outlet stemming mainly from machining imperfections. Wall roughness provides the nucleation sites necessary for cavitation to arise in the outlet part of the injector and cavitation is sustained by the low pressure prevailing in the region. The supplementary video (SV_D) also highlights the onset of transient vaporous structures in the vicinity of the nozzle outlet. It must also be pointed out here that a schlieren visualisation for the Spray D layout is available in the Supplementary material (SV_D_Schlieren), where longitudinal structures are evident to emanate from the needle tip and propagate through to the nozzle hole. It was preferred not to add a sequence of schlieren images in Fig. 4 since the relative refractive index gradients are quite challenging to discern in still images.

Since the injection duration depends on the injection pressure, the non-dimensional time parameter t*, which is time over total injection time ($t^*=t/t_{total}$) is introduced to make comparison more straightforward for different conditions.

Post-processing of high-speed images throughout the injection event enabled the calculation of vapour presence probability and relevant standard deviation, as depicted in Fig. 5 for the Spray C injector. The straight injector-hole layout causes Spray C to cavitate heavily, with the entire nozzle being filled with vapour almost for the entirety of the injection, as illustrated by the mean probability values. It must be pointed out that this doesn't necessarily mean that the entire orifice volume is filled with vapour but rather that an external layer shrouds the wall periphery, thus preventing light from penetrating further. The locally high standard deviation values suggest the presence of transient cavities in the core region. The presence of transient vaporous structures is demonstrated more clearly in the images corresponding to the additised sample. As can be seen, a slender region of low mean probability values

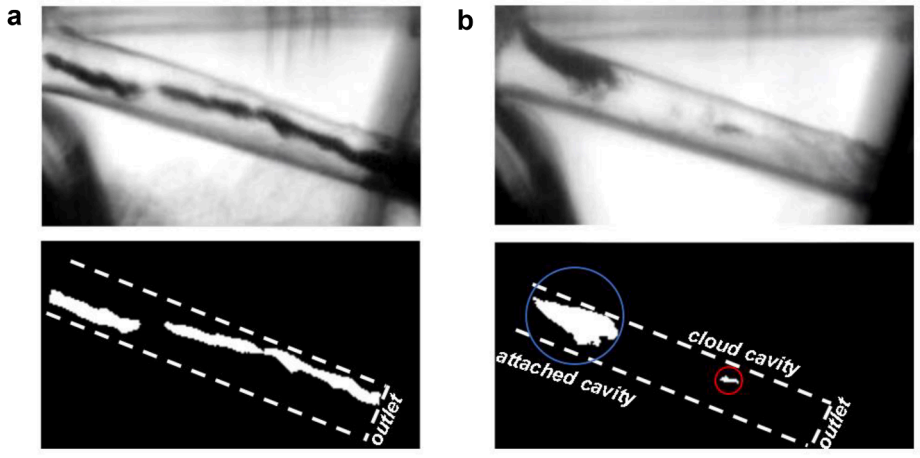

Fig. 3. Detection of cloud and vortical cavitation in the Spray-M injector: (a) Case of well-established elongated cavity identified by the eccentricity criterion, (b) case of both attached and vortical cavities identified through a combination of eccentricity and location criteria.

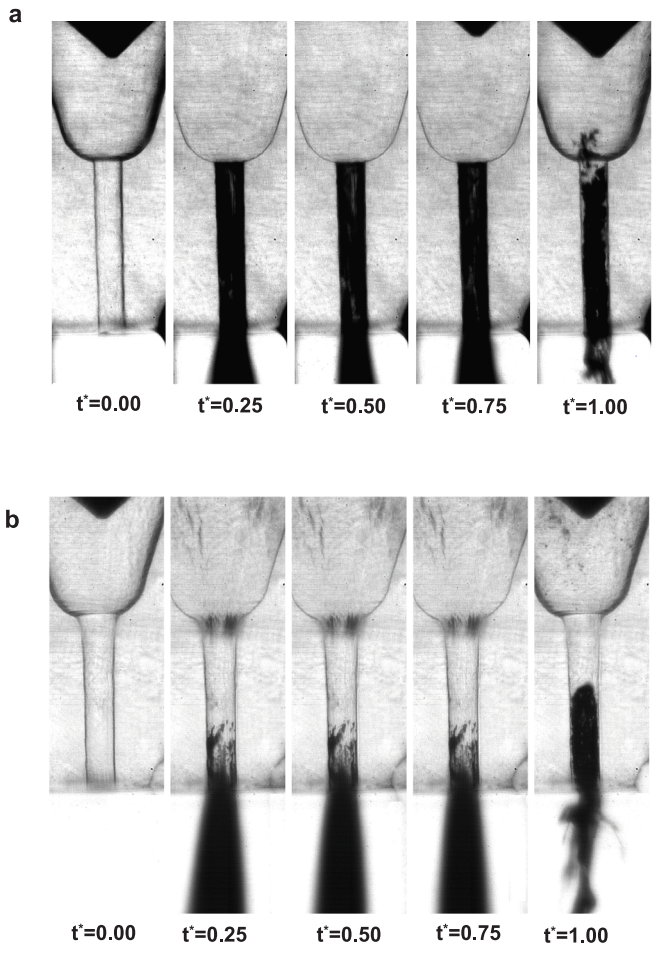

Fig. 4. An indicative sequence of raw images covering the entire injection event for the cases of the single-hole injectors: (a) Spray C for injection and ambient pressures of 700 and 5 bar and (b) Spray D for 900 and 5 bar, respectively. The hydraulic injection duration is different for the two layouts, despite the identical electric pulse, owing to the different injection pressures and is therefore presented in a non-dimensional form.

can be detected, where the respective standard deviation obtains its maximum values. A visual impression of the evolution of transient cavities is also given by the animation of raw images for the additised sample (SV_C_addi) provided as Supplementary material.

Based on the binarised images, the vapour projected area has been measured for each frame and its distribution with time for the entire injection event is plotted in Fig. 6. The three panels of Fig. 6 correspond to increasing values of back pressure and, thus, decreasing CN values. Similar trends can be observed in all graphs, with the base sample exhibiting the highest projected area values and the biodiesel samples the lowest ones, respectively. The underlying cause should be sought for the difference in thermophysical properties, namely viscosity and saturation pressure, subsequently modifying the Reynolds number and CN. It is interesting to notice that the tested QAS additised sample consistently exhibits lower cavitation projected-area values than the reference diesel, although their thermodynamic and transport properties are identical for the specific concentration of polymeric additive [54]. The discrepancy in this case, must be attributed to fuel rheology. As discussed in previous studies from the authors' group [53], the QAS additives form flexible micelles, once diluted in the base fuel [48]. These micelles interact with vortices at different length scales, i.e., coherent vortical motion and turbulence, eventually influencing the cavitation formation processes, yet in a manner dependent on the cavitation regime. Experiments in injector enlarged replicas utilising XPCI [54] have shown that viscoelastic fuels exhibit smaller amounts of attached cavitation compared to Newtonian diesel samples [49]. This conclusion seems to be confirmed in real injector devices, as well.

Fig. 7 depicts the distribution of spray cone angle with time for Spray C in a comparative manner for the three fuel samples examined. In general, increasing back-pressure leads to higher cone angles, owing to aerodynamic effects, i.e., drag forces, which become the prevalent effect for 20 bar ambient pressure (Fig. 8c); this is a well-known finding [63]. On average, the biodiesel sample exhibits the lowest cone-angle values compared to the other two samples, which is expected due to its increased viscosity [32]. It is interesting to notice that the additised sample exhibits considerably higher peak values than the base diesel in all examined cases. The micro-schlieren technique implemented has demonstrated that the increased cone angle is associated with the presence of longitudinal vortices within the injector hole [7], which gives rise to elongated cavities as well. Moreover, it is known that a prevalent effect of viscoelasticity on wall-bounded flows is turbulence suppression [64,65]. Turbulence, or in other words, small-scale eddies, leads to the decay of large-scale vortices due to viscous damping. Hence,

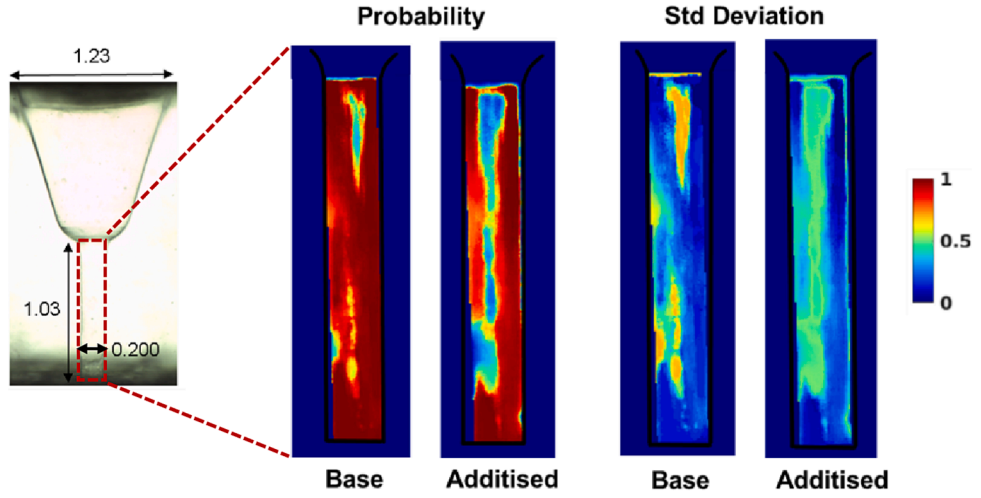

Fig. 5. Vapour presence probability and respective standard deviation within the straight Spray C injector. Contour plots correspond to base fuel and ambient pressure of 5 bar. The black line indicates the outline of the injector-hole straight part. Cavitation does not appear in the sac region for the Spray C injector. All dimensions in the schematic are in mm.

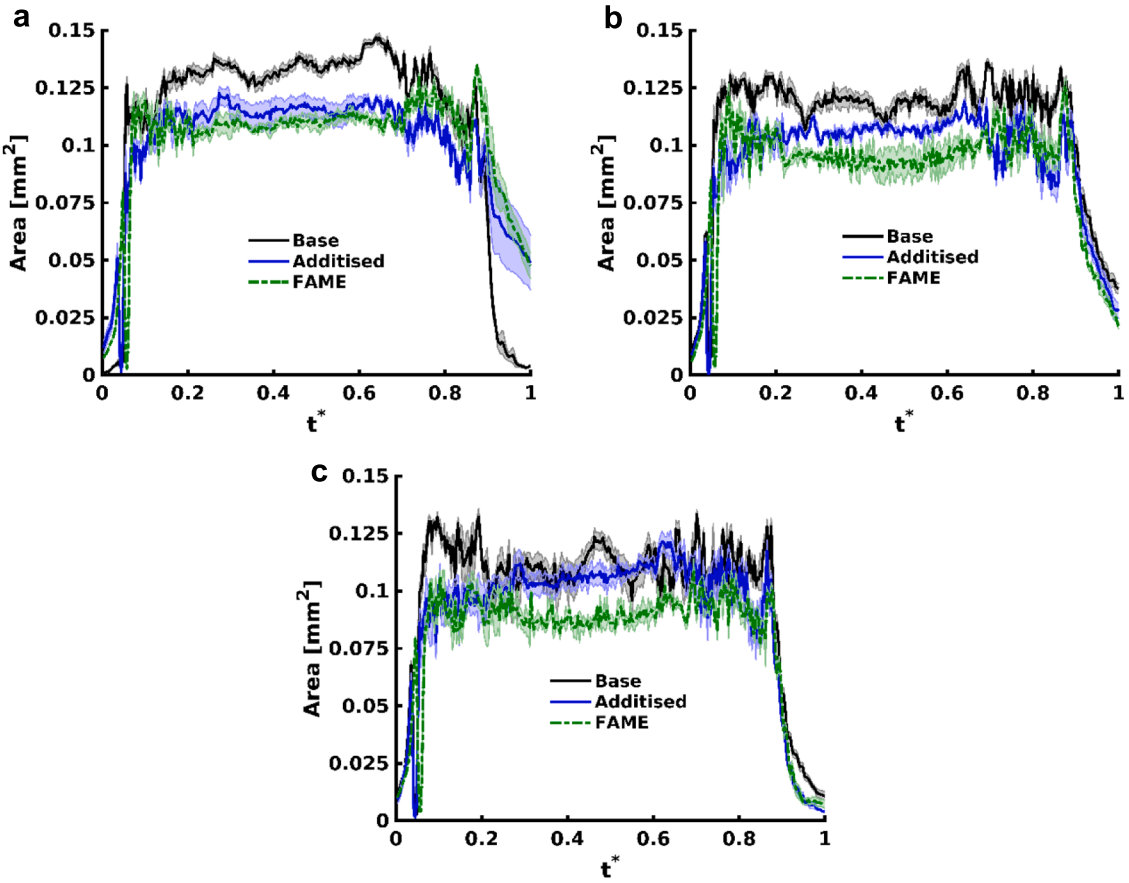

Fig. 6. Distribution of the projected cavitation area with time in the Spray C injector for ambient pressures of (a) 1 bar, (b) 5 bar and (c) 20 bar. The duration of the injection event in absolute values is 311 ms. The shade of the same colour encompassing each graph line corresponds to standard statistical error.

reduced turbulence favours the prevalence of elongated vortices, a postulation in agreement with the experimental results for the additised sample.

Fig. 8 presents contour plots of the same quantities as Fig. 5, however for the Spray D injector. It is evident that vapour formation is suppressed in this device due to its tapered layout and hydro-grinded entrance. Static attached cavities can be seen in the entrance region, whereas transient cavities emerge towards the orifice outlet, as confirmed by the relatively high standard deviation values stemming mainly from machining imperfections [7]. The major part of the injector hole is occupied by pure liquid, while cavitation is completely absent from the sac region as well.

In a similar manner to Fig. 6, Fig. 9 presents the same distribution, yet for the Spray D tip and ambient conditions of 5 and 20 bar. The injection pressure is maintained at 900 bar. Once again, regardless of the ambient pressure, the biodiesel sample exhibits the lowest projected-area values. An additional observation that can be made is that at approximately $t^* = 0.7$, both base and additised fuels show a local decrease in cavitation area, while the opposite is true for FAME regardless of the ambient pressure. Reduced in-nozzle level of turbulence (due to increased viscosity) for the biodiesel sample could potentially lead to higher lifetime of the vortical cavities at the closing stage of the injection event, where transient cavities do arise. The hydraulic characteristics of the injection, e.g., needle wobble, are also modified by fuel viscosity (as also demonstrated by the variance in injection duration) and could also contribute to the prevalence of vortical cavitation of slightly different morphology between the cases of base/additised diesel and biodiesel.

Besides, it is interesting to notice that the additised sample shows a non-consistent trend compared to the reference fuel. For the 5-bar ambient pressure case (Fig. 9a), the two fuels have nearly identical distributions, yet with the viscoelastic fuel exhibits slightly lower projected area values. The trend is reversed for a 20-bar ambient (Fig. 9b, where CN actually decreases). A plausible underlying cause is discussed in relevance to Fig. 9, although the relevant differences are admittedly on the verge of experimental uncertainty.

Fig. 10a depicts the averaged presence probability of refractive index gradients corresponding to vortical structures within the nozzle throughout the duration of the injection event, as well as the respective standard deviation. Schlieren imaging was made possible in the mildly-cavitating Spray D injector, where optical access to the nozzle could be attained. The probability contours plots illustrate the highly transient nature of the longitudinal vortices, as maximum probability is of the order of 10 %. The standard-deviation plot indicates that structures forming in the sac region and in the vicinity of the needle tip, are subsequently entrained in the injector hole. Fig. 9b quantifies the temporally-averaged projected area of vortical structures for different ambient conditions and fuel samples. The biodiesel fuel exhibits the lowest values due to enhanced viscous damping of the structures. Besides, the additised sample obtains a comparable averaged value to the base diesel for 5-bar ambient pressure case, yet it retains this value, despite the increase of the ambient pressure, unlike the reference counterpart. This behaviour is indicative of the enhancement of longitudinal vortices under the presence of viscoelastic additives, with subsequent after-effects in vortical cavitation, as shown in Fig. 10b, and is in agreement with past studies [54,66].

The distribution of spray cone angle with time for Spray D is shown in Fig. 11. As can be seen, no appreciable differences can be detected between the base and additised samples due to the less-perturbed flow prevailing within the injector nozzle. The biodiesel sample follows a

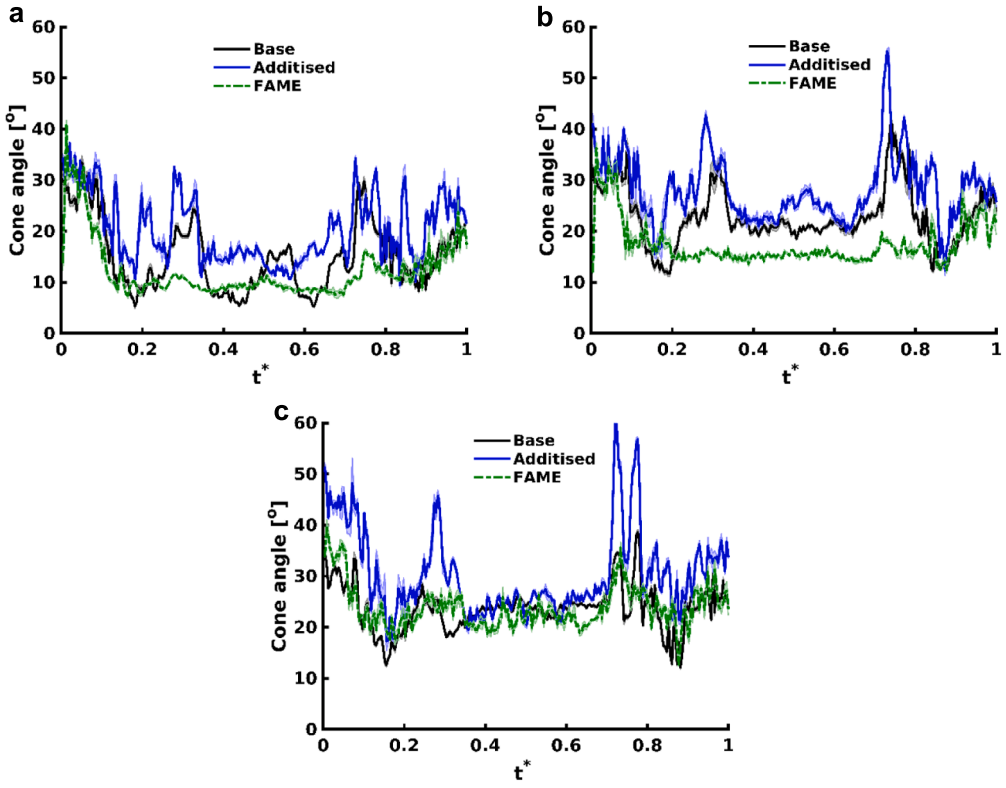

Fig. 7. Distribution of the spray cone angle with time for the Spray C injector and ambient pressures of (a) 1 bar, (b) 5 bar and (c) 20 bar.

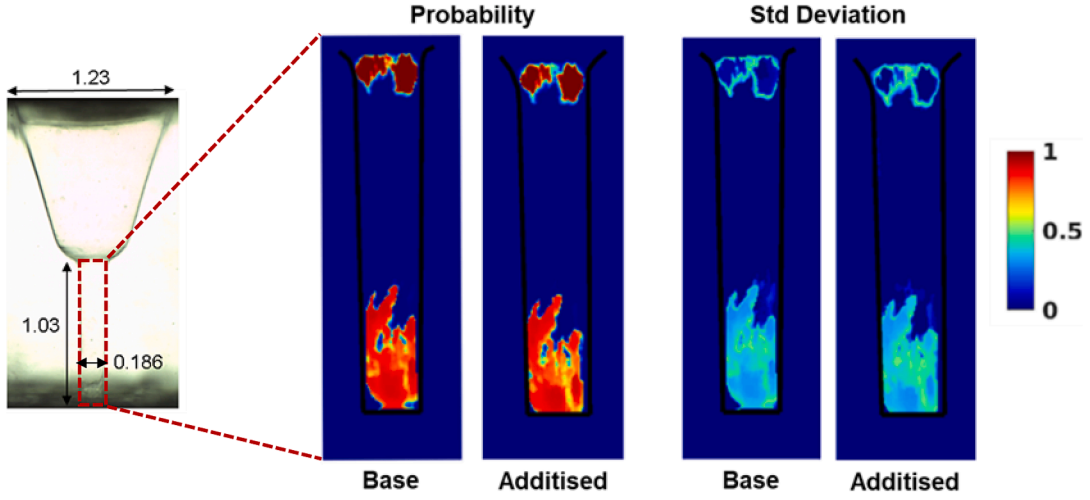

Fig. 8. Vapour presence probability and respective standard deviation within the tapered Spray D injector. Contour plots correspond to base fuel and ambient pressure of 5 bar. The black line indicates the outline of the injector-hole straight part. Cavitation does not appear in the sac region for the Spray D injector.

behaviour similar to the Spray C nozzle, with lower values than the two other samples (Fig. 11a) for the 5-bar ambient and relatively comparable values, denoting the primary influence of drag forces for ambient pressure of 20 bar.

3.2. Multi-hole injector Spray M

Spray M experiments were carried out at ambient pressures of 5 bar and 20 bar with an injection pressure of 500 bar. Fig. 12, along with the supplementary animation SV_M, depict time sequences of raw DBI images and clearly underpin the highly transient nature of cavitation arising in the multi-hole injector. A dedicated injector hole of interest located perpendicular to the line of sight is visualised, while the injected spray plumed from the other nozzles do not hinder visualisation, as they are drained through the dedicated ducts realised in the pedestal. During most of the event period, the hole of interest is occupied by pure liquid with incipient cavitation structures arising infrequently. However, short-lived yet coherent vortical cavities can also be detected, as can be seen at time instances t*=0.12 and 0.13 of Fig. 12.

Similar to single-hole nozzles, vapour presence probability and standard deviation within the Spray M injector was obtained by averaging the post-processed images throughout the injection event. Indicative contour plots for the visualised nozzle hole and base fuel are presented in Fig. 13 Maximum probability is of the order of 5 %

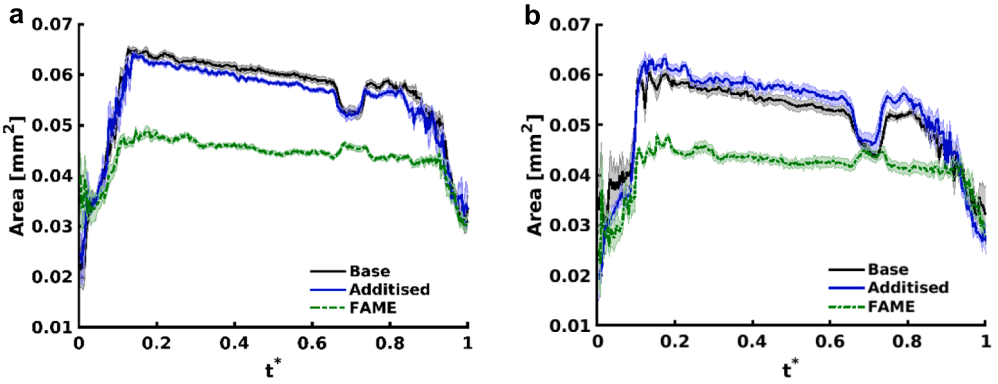

Fig. 9. Distribution of the projected cavitation area with time for the Spray D injector and ambient pressures of (a) 5 bar, (b) 20 bar. The duration of the injection event in absolute values is 267 ms.

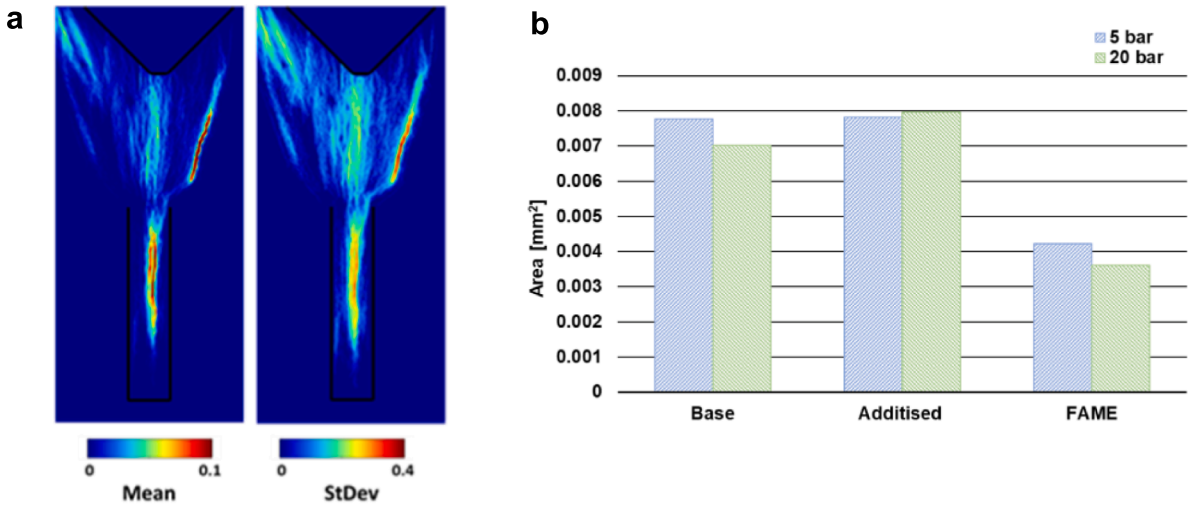

Fig. 10. (a) Contour plots of vortical-structures mean presence probability and standard deviation in the Spray D injector (base fuel, 900/5 bar); (b) Temporally-averaged projected area of vortical structures for different ambient conditions.

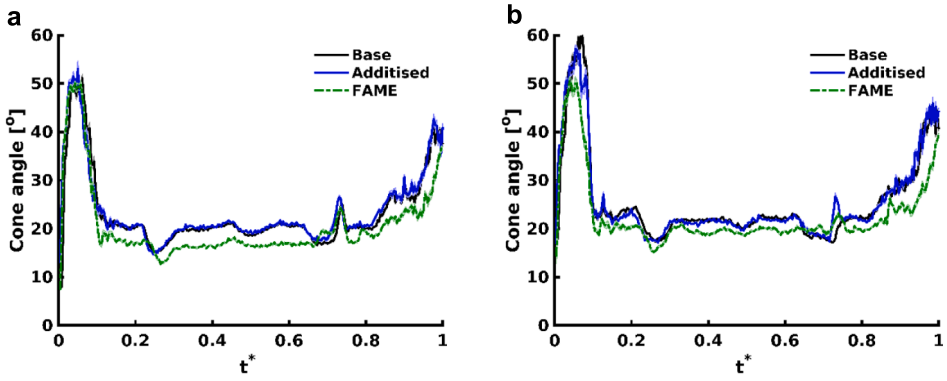

Fig. 11. Distribution of the spray cone angle with time in the Spray D injector for ambient pressures of (a) 5 bar, (b) 20 bar.

(Fig. 13a), which is illustrative of the highly transient cavitation evolution in the specific layout, as also demonstrated by the high-standard deviation values prevailing throughout the orifice length (Fig. 13b). It can also be discerned from the plots of Fig. 13 that the high vapour-probability regions are located in the orifice core and have an elongated shape characteristic of cavities manifesting due to the presence of longitudinal vortices.

In conformity to Fig. 7 and 11, the distribution of spray cone angle with time for Spray M is shown in Fig. 14. The expected trend of increasing time-averaged cone angle with ambient pressure is once again verified, for instance from 43.8° to 52.5° for the base sample. Besides, the biodiesel sample exhibits on average a smaller cone angle compared to the base and additised samples, equal to 34° and ~45° for the 5 and 20 bar pressures, respectively. The influence of vortical cavitation is highlighted by the fluctuating cone angle even between t* of 0.2 and 0.8 during which the needle valve has reached its maximum

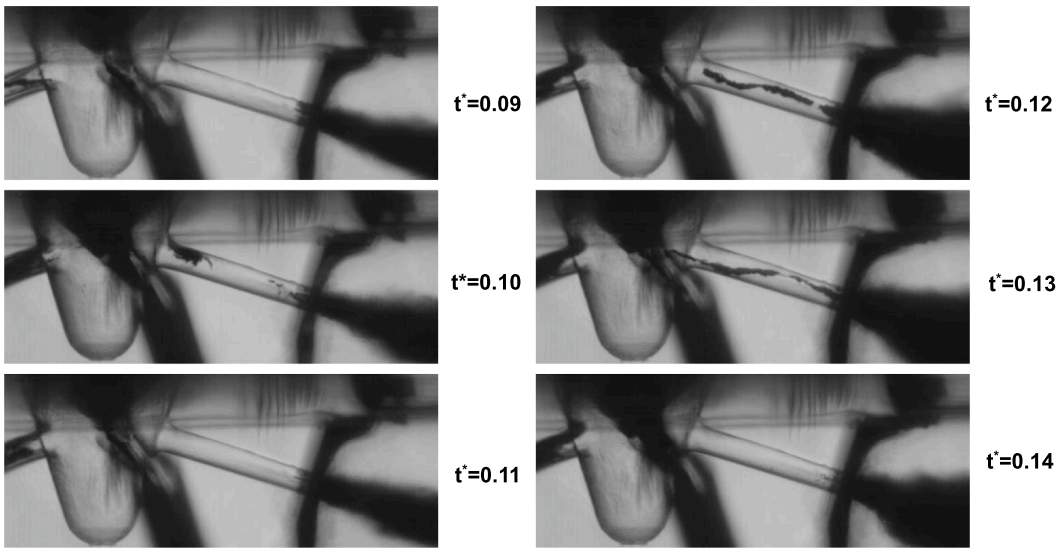

Fig. 12. An indicative sequence of raw images for the Spray M injector. Cavitation is manifested primarily in the form of transient structures; hence the images were selected in such a manner to capture the formation of cloud and vortical cavities.

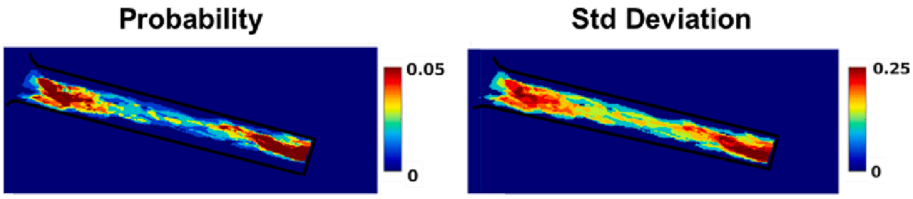

Fig. 13. Vapour presence probability and respective standard deviation within the multi-hole Spray M injector. Contour plots correspond to base fuel and ambient pressure of 5 bar. The black line corresponds to the outline of the 'active' injector-hole for visualisation.

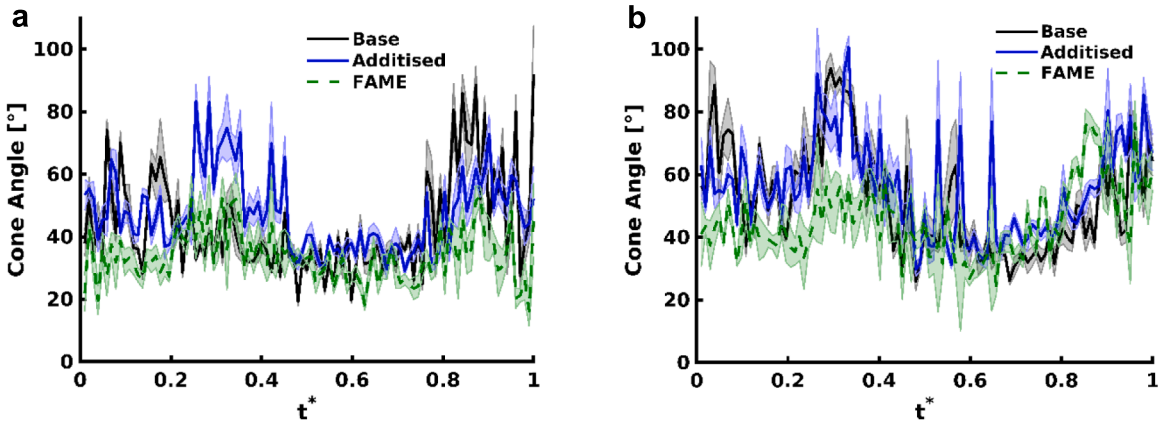

Fig. 14. Distribution of the spray cone angle with time in the Spray M injector for ambient pressures of (a) 5 bar and (b) 20 bar.

positions and remains still. Distinct peaks appear in the distributions for both 5 bar (Fig. 14a, between 0.2. and 0.4) and 20 bar ambient (Fig. 14b, between 0.2 and 0.6) pressures, which are linked to the manifestation of coherent vortical cavities within the injector hole that prevail all the way to the outlet, as also observed in [7]. Overall, the additised sample exhibits the highest average cone-angle values equal to 47.5° and ~ 55.5° for the low- and high-pressure environment, respectively, a trend which can also serve as an indication of enhanced vortex coherence close to the injector outlet.

The total cavitation projected area within the Spray M nozzle for the two ambient pressures examined is presented in Fig. 15. The bar charts of Fig. 15 were created by integrating the projected area of vaporous structures detected throughout the duration of the injection event. The projected area decreases with increasing ambient pressure, as expected; the biodiesel sample exhibits smaller values. These observations are linked to the non-dimensional numbers designating the flow conditions, as, for instance, increased ambient pressure decreases CN, while high viscosity leads to a decrease of the Reynolds number, both of which lead to reduced cavitation. It is also important to notice that the additised sample exhibits a smaller extent of in-nozzle cavitation compared to base diesel for both ambient pressures.

In order to explain this trend, firstly, it must be clarified that in

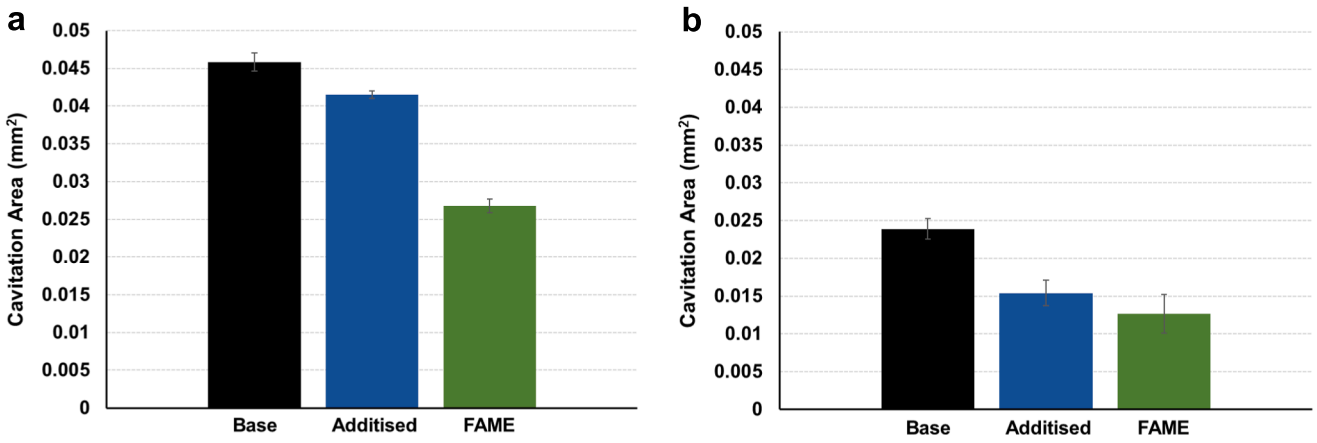

Fig. 15. Total cavitation projected area in the visualised injector hole of Spray M for ambient pressures of (a) 5 and (b) 20 bar. Area has been integrated over the entire injection duration.

previous works of the authors' group performed in enlarged diesel-injector replicas, it was found that longitudinal cavities gained in coherence owing to viscoelasticity [37,38,48]. The postulated mechanism stated that the reduction of the overall level of turbulence, a well-established effect of viscoelastic additives, also reduces viscous damping. However, in the current experiments, string-like vortices do not obtain a stable behaviour yet have lifetimes of only a few μs, also owing to flow instabilities induced by the transient needle motion. In other words, the main findings of the current study should be compared against the respective referring to gasoline injection in realistic optical devices with transient needle motion, reported in [57], where the manifestation of transient vortical cavities is also suppressed in additised gasoline samples.

Fig. 16 depicts the number of individual elongated structures detected, based on the post-processing criteria set, throughout the injection for the examined fuels. The trends exhibited seem to corroborate with the already established conclusions. For both ambient pressures, fewer string cavities emerge in the injector hole for the additised sample, with the difference compared to base fuel being more substantial for the 20-bar ambient (Fig. 16b), for which CN is also reduced. In other words, reduced flow turbulence as an after effect of additive action leads to less extensive vortex roll-up and, thus, lesser cavitation formation. It is interesting to notice that the decreasing trend in the absolute number of strings correlates with that of the overall projected cavitation area of Fig. 15, an additional indication that vortical cavitation is the prevailing regime in the Spray M layout. The smallest numbers of string cavities during injection are encountered for the biodiesel sample, once again an expected result due to its thermophysical properties, which nevertheless serves as further evidence for the validity of the post-processing method.

4. Conclusions

This study employed diffuse-backlight illumination and micro-schlieren high-speed imaging to shed light on the cavitation patterns arising in the internal flow path of single-hole and multi-hole transparent diesel injectors, as well as on the near-nozzle spray dynamics. Emphasis was placed on viscoelastic effects induced by QAS additives diluted in base diesel which were compared against the equivalent visualisation obtained with the Newtonian standard diesel and biodiesel fuels (FAME). The comparative assessment has demonstrated that the sample treated with viscoelastic additives exhibits a reduced extent of geometrical, wall-attached cavitation compared to the base counterpart in the heavily cavitating straight-orifice design examined despite their identical physical properties.

In accordance with previous studies obtained in enlarged nozzle replicas, it has been proven that viscoelasticity tends to suppress flow instabilities, i.e., turbulence, in the injector hole. Well-established, steady vortices as those prevailing in the single-hole injectors have been proven to be enhanced by this effect, while, on the contrary, the manifestation of highly transient vortices and, thus, cavities in the multi-hole Spray M injector is hindered. With respect to spray topology, the additised sample has consistently shown higher cone angles compared to

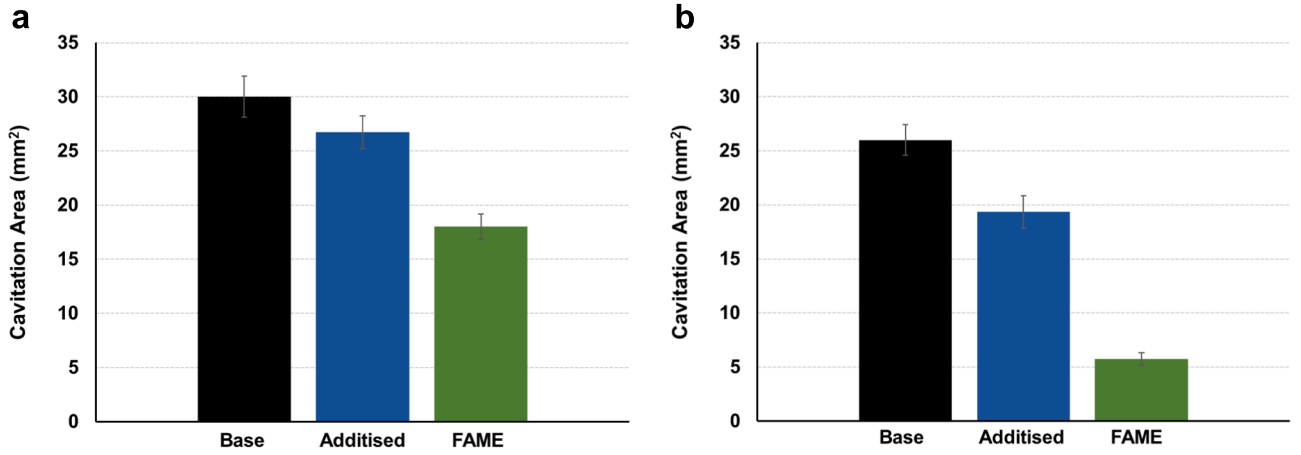

Fig. 16. Number of discrete vortical cavities detected over the injection event in the Spray-M injector hole at (a) 5 and (b) 20 bar ambient pressures.

base diesel, under well-established cavitation conditions, presumably due to the enhancement of vortical cavitation, as demonstrated by the schlieren visualisation. The biodiesel fuel sample exhibited the smallest in-nozzle extent of cavitation and smaller spray divergence for all injector configurations owing to its higher viscosity and saturation pressure compared to the other two samples. The key takeaway message of the present investigation is that fuel treatment with additives of suitable chemistry to induce a weakly viscoelastic nature can enhance both the injector performance and reliability by enhancing in-nozzle vortical motion; this is closely linked to spray atomisation and suppressing near-wall bubble formation and therefore collapse that can lead to material erosion.

CRediT authorship contribution statement

Onur Baran: Conceptualization, Data curation, Formal analysis, Investigation, Methodology, Software, Visualization, Writing – original draft. **Ioannis K. Karathanassis:** Conceptualization, Data curation, Formal analysis, Funding acquisition, Investigation, Methodology, Supervision, Visualization, Writing – review & editing. **Phoevos Koukouvinis:** Conceptualization, Data curation, Formal analysis, Investigation. **Joonsik Hwang:** Data curation, Investigation, Methodology, Writing – review & editing. **Lyle M. Pickett:** Conceptualization, Formal analysis, Investigation, Writing – review & editing. **David Spivey:** Conceptualization, Investigation, Writing – review & editing. **Manolis Gavaises:** Conceptualization, Funding acquisition, Supervision, Writing – review & editing.

Declaration of Competing Interest

The authors declare the following financial interests/personal relationships which may be considered as potential competing interests: Onur Baran reports financial support was provided by European Commission Marie Sklodowska-Curie Actions. Ioannis Karathanassis reports financial support was provided by European Commission Marie Sklodowska-Curie Actions. Phoevos Koukouvinis reports was provided by European Commission Marie Sklodowska-Curie Actions. David Spivey reports a relationship with Lubrizol Ltd that includes: employment.

Data availability

Data will be made available on request.

Acknowledgements

This Article has been co-authored by National Technology and Engineering Solutions of Sandia, LLC. under contract No. DE-NA0003525 with the U.S. Department of Energy/National Nuclear Security Administration. The United States Government retains and Elsevier, by accepting the article for publication, acknowledges that the United States Government retains a non-exclusive, paid-up, irrevocable, worldwide license to publish or reproduce the published form of this manuscript, or allow others to do so, for United States Government purposes. The work was performed at the Combustion Research Facility (CRF), Sandia National Laboratories, Livermore, CA, with support from the Spray Combustion Consortium and the DOE Office of Vehicle Technologies. Funding from the EU Horizon-2020 Marie Skłodowska-Curie Global Fellowships AHEAD (IK, Grant No. 794831) and UNIFIED (PK, Grant No. 748784) is acknowledged, which also supported the international visiting program of Ioannis K. Karathanassis and Phoevos Koukouvinis at the Sandia National Laboratories. This work has received funding from the European Union Horizon 2020 Research and Innovation programme under the Marie Sklodowska-Curie grant agreement No. 861002 (EDEM project). Additional funding has been received by the UK's Engineering and Physical Sciences Research Council (EPSRC) through grant EP/K020846/1.

Appendix A. Supplementary data

Supplementary data to this article can be found online at https://doi.org/10.1016/j.fuel.2023.129076.

References

[1] Bloomberg NEF, "Electric vehicle Outlook BNEF," 2022.
[2] E. Commission, "Euro 7 Standards," 2022.
[3] Gavaises M. Flow in valve covered orifice nozzles with cylindrical and tapered holes and link to cavitation erosion and engine exhaust emissions. Int J Engine Res 2008;9(6):435–47. https://doi.org/10.1243/14680874JER01708.
[4] Manin J, Pickett LM, Yasutomi K. Transient cavitation in transparent diesel injectors. In: ICLASS 2018–14th International Conference on Liquid Atomization and Spray Systems; 2020. p. 1–9.
[5] R. Balz, A. Schmid, and D. Sedarsky, "In-Nozzle Flow Visualization of Marine Diesel Injector Nozzles with Different Inlet Radii," *Proceedings of the 10th International Symposium on Cavitation (CAV2018)*, pp. 567–571, 2019, doi: 10.1115/1.861851_ch108.
[6] Abers PM, Cenker E, Yasutomi K, Hwang J, Pickett LM. Effect of pressure cycling on gas exchange in a transparent fuel injector. SAE TechPapers 2019:1–11. https://doi.org/10.4271/2019-01-2280.
[7] Karathanassis IK, Hwang J, Koukouvinis P, Pickett L, Gavaises M. Combined visualisation of cavitation and vortical structures in a real-size optical diesel injector. Exp Fluids 2021;62(1). https://doi.org/10.1007/s00348-020-03096-1.
[8] Desantes JM, Pastor JV, Payri R, Pastor JM. Experimental characterization of internal nozzle flow and diesel spray behavior. Part I: Non Evaporative conditions. Atomization Sprays 2005;15(5):517–43. https://doi.org/10.1615/atomizspr.v15.i5.30.
[9] Mitroglou N, McLorn M, Gavaises M, Soteriou C, Winterbourne M. Instantaneous and ensemble average cavitation structures in Diesel micro-channel flow orifices. Fuel 2014;116:736–42. https://doi.org/10.1016/j.fuel.2013.08.060.
[10] N. Mitroglou, M. Gavaises, and D. Arcoumanis, *Spray stability from VCO and a new diesel nozzle design concept*. Woodhead Publishing Limited, 2012. doi: 10.1533/9780857096043.7.279.
[11] Gavaises M, Murali-Girija M, Rodriguez C, Koukouvinis P, Gold M, Pearson R. Numerical simulation of fuel dribbling and nozzle wall wetting. Int J Engine Res 2022;23(1):132–49. https://doi.org/10.1177/1468087420985189.
[12] Koukouvinis P, Gavaises M, Li J, Wang L. Large Eddy Simulation of Diesel injector including cavitation effects and correlation to erosion damage. Fuel 2016;175:26–39. https://doi.org/10.1016/j.fuel.2016.02.037.
[13] Mithun MG, Koukouvinis P, Gavaises M. Numerical simulation of cavitation and atomization using a fully compressible three-phase model. Phys Rev Fluids 2018;3(6):1–27. https://doi.org/10.1103/PhysRevFluids.3.064304.
[14] Cristofaro M, Edelbauer W, Koukouvinis P, Gavaises M. A numerical study on the effect of cavitation erosion in a diesel injector. Appl Math Model 2020;78:200–16. https://doi.org/10.1016/j.apm.2019.09.002.
[15] Koukouvinis P, Mitroglou N, Gavaises M, Lorenzi M, Santini M. Quantitative predictions of cavitation presence and erosion-prone locations in a high-pressure cavitation test rig. J Fluid Mech 2017;819:21–57. https://doi.org/10.1017/jfm.2017.156.
[16] Kolovos K, Koukouvinis P, McDavid RM, Gavaises M. Transient cavitation and friction-induced heating effects of diesel fuel during the needle valve early opening stages for discharge pressures up to 450 MPa. Energies 2021;14(10):2923.
[17] Reid BA, Gavaises M, Mitroglou N, Hargrave GK, Garner CP, Long EJ, et al. On the formation of string cavitation inside fuel injectors. Exp Fluids 2014;55(1). https://doi.org/10.1007/s00348-013-1662-8.
[18] Manin J, Pickett LM, Yasutomi K. Stereoscopic high-speed microscopy to understand transient internal flow processes in high-pressure nozzles. Exp Therm Fluid Sci 2020;114:110027. https://doi.org/10.1016/j.expthermflusci.2019.110027.
[19] Duke D, Swantek A, Tilocco Z, Kastengren A, Fezzaa K, Neroorkar K, et al. X-ray imaging of cavitation in diesel injectors. SAE Int J Engines 2014;7(2):1003–16.
[20] Moon S, Huang W, Wang J. First observation and characterization of vortex flow in steel micronozzles for high-pressure diesel injection. Exp Therm Fluid Sci 2019;105:342–8. https://doi.org/10.1016/j.expthermflusci.2019.04.018.
[21] Andriotis A, Gavaises M, Arcoumanis C. Vortex flow and cavitation in diesel injector nozzles. J Fluid Mech 2008;610:195–215. https://doi.org/10.1017/S0022112008002668.
[22] Chen Z, He Z, Shang W, Duan L, Zhou H, Guo G, et al. Experimental study on the effect of nozzle geometry on string cavitation in real-size optical diesel nozzles and spray characteristics. Fuel 2018;232:562–71.
[23] Gavaises M, Papoulias D, Andriotis A, Giannadakis E, Theodorakakos A. Link between cavitation development and erosion damage in diesel injector nozzles. SAE Tech Pap 2007;2007(724):776–90. https://doi.org/10.4271/2007-01-0246.
[24] Gomez Santos E, Shi J, Gavaises M, Soteriou C, Winterbourn M, Bauer W. Investigation of cavitation and air entrainment during pilot injection in real-size multi-hole diesel nozzles. Fuel 2020;263:116746. https://doi.org/10.1016/j.fuel.2019.116746.
[25] C. Arcoumanis, H. Flora, M. Gavaises, and M. Badami, "Cavitation in real-size multi-hole diesel injector nozzles," *SAE Technical Papers*, no. 724, 2000, doi: 10.4271/2000-01-1249.

[26] Hayashi T, Suzuki M, Ikemoto M. Effects of internal flow in a diesel nozzle on spray combustion. Int J Engine Res 2013;14(6):646–54. https://doi.org/10.1177/1468087413494910.
[27] Wei M, Gao Y, Yan F, Chen L, Feng L, Li G, et al. Experimental study of cavitation formation and primary breakup for a biodiesel surrogate fuel (methyl butanoate) using transparent nozzle. Fuel 2017;203:690–9.
[28] P. Dong, K. Nishida, and Y. Ogata, "Characterization of multi-hole nozzle sprays and internal flow for different nozzle hole lengths in direct-injection diesel engines," *Proceedings of the Institution of Mechanical Engineers, Part D: Journal of Automobile Engineering*, vol. 231, no. 4, pp. 500–515, 2017, doi: 10.1177/0954407016653890.
[29] Huang W, Moon S, Gao Y, Wang J, Ozawa D, Matsumoto A. Hole number effect on spray dynamics of multi-hole diesel nozzles: an observation from three- to nine-hole nozzles. Exp Therm Fluid Sci 2019;102:387–96. https://doi.org/10.1016/j.expthermflusci.2018.12.022.
[30] Cao T, He Z, Zhou H, Guan W, Zhang L, Wang Q. Experimental study on the effect of vortex cavitation in scaled-up diesel injector nozzles and spray characteristics. Exp Therm Fluid Sci 2020;113:110016. https://doi.org/10.1016/j.expthermflusci.2019.110016.
[31] Yasutomi K, Hwang J, Pickett LM, Sforzo B, Matusik K, Powell CF. Transient internal nozzle flow in transparent multi-hole diesel injector. SAE Tech Papers 2020. https://doi.org/10.4271/2020-01-0830.
[32] Chang CT, Farrell PV. A study on the effects of fuel viscosity and nozzle geometry on high injection pressure diesel spray characteristics. SAE Tech Papers 1997;106:558–67. https://doi.org/10.4271/970353.
[33] Desantes JM, Arrègle J, Pastor JV, Delage A. Influence of the fuel characteristics on the injection process in a D.I Diesel engine. SAE Tech Papers 1998;724. https://doi.org/10.4271/980802.
[34] Rokni HB, Moore JD, Gupta A, McHugh MA, Gavaises M. Entropy scaling based viscosity predictions for hydrocarbon mixtures and diesel fuels up to extreme conditions. Fuel 2019;241:1203–13.
[35] Rowane AJ, Mallepally RR, Gavaises M, McHugh MA. Interfacial tension of isomers n-hexadecane and 2,2,4,4,6,8,8- heptamethylnonane with nitrogen at high pressures and temperatures. Ind Eng Chem Res 2020;59(19):9293–9. https://doi.org/10.1021/acs.iecr.0c00213.
[36] Rowane AJ, Gupta A, Gavaises M, McHugh MA. Experimental and modeling investigations of the phase behavior and densities of diesel + nitrogen mixtures. Fuel 2020;265:117027. https://doi.org/10.1016/j.fuel.2020.117027.
[37] Rowane AJ, Gavaises M, McHugh MA. Vapor-liquid equilibria and mixture densities for 2,2,4,4,6,8,8-heptamethylnonane + N2 and n-hexadecane + N2 binary mixtures up to 535 K and 135 MPa. Fluid Phase Equilib 2020;506:112378. https://doi.org/10.1016/j.fluid.2019.112378.
[38] Rowane AJ, Mahesh Babu V, Rokni HB, Moore JD, Gavaises M, Wensing M, et al. Effect of composition, temperature, and pressure on the viscosities and densities of three diesel fuels. J Chem Eng Data 2019;64(12):5529–47.
[39] Rowane AJ, Mallepally RR, Gupta A, Gavaises M, Mchugh MA. High temperature, high-pressure viscosities and densities of n-hexadecane, 2,2,4,4,6,8,8-heptamethylnonane, and squalane measured using a universal calibration for a rolling-ball viscometer/densimeter. Ind Eng Chem Res 2019;58(10):4303–16. https://doi.org/10.1021/acs.iecr.8b05952.
[40] Rokni HB, Gupta A, Moore JD, McHugh MA, Bamgbade BA, Gavaises M. Purely predictive method for density, compressibility, and expansivity for hydrocarbon mixtures and diesel and jet fuels up to high temperatures and pressures. Fuel 2019;236:1377–90.
[41] Rokni HB, Moore JD, Gavaises M. Entropy-scaling based pseudo-component viscosity and thermal conductivity models for hydrocarbon mixtures and fuels containing iso-alkanes and two-ring saturates. Fuel 2021;283:118877.
[42] Vidal A, Kolovos K, Gold MR, Pearson RJ, Koukouvinis P, Gavaises M. Preferential cavitation and friction-induced heating of multi-component Diesel fuel surrogates up to 450MPa. Int J Heat Mass Transf 2021;166:120744. https://doi.org/10.1016/j.ijheatmasstransfer.2020.120744.
[43] Mo J, Tang C, Li J, Guan L, Huang Z. Experimental investigation on the effect of n-butanol blending on spray characteristics of soybean biodiesel in a common-rail fuel injection system. Fuel 2016;182:391–401. https://doi.org/10.1016/j.fuel.2016.05.109.
[44] Birgel A, et al. Deposit formation in the holes of diesel injector nozzles: a critical review. SAE Tech Papers 2008. https://doi.org/10.4271/2008-01-2383.
[45] Owen K, Coley T. Automotive Fuels Reference Book. SAE; 1995.
[46] S. K. Puri *et al.*, "SYNERGISTIC DEPOSIT CONTROL ADDITIVE COMPOSITION FOR DIESEL FUEL AND PROCESS THEREOF," 2006/0277819 A1, 2006.
[47] R. Barbour, "Method to provide power gain in an engine," *US Patent Number US9239000*, vol. 2, no. 12, 2011.
[48] A. F. Sarofim and A. B. Palotas, "Combustion Science and Technology EVALUATION OF ORGANOMETALLIC FUEL ADDITIVES FOR SOOT SUPPRESSION," no. February 2013, pp. 987–1001, 2010.
[49] Miyamoto N, Ogawa H, Nurun NM, Obata K, Arima T. Smokeless, Low NOx, high thermal efficiency, and low noise diesel combustion with oxygenated agents as main fuel. SAE Tech Papers 1998;724. https://doi.org/10.4271/980506.
[50] Mueller CJ, Pitz WJ, Pickett LM, Martin GC, Siebers DL, Westbrook CK. Effects of oxygenates on soot processes in di diesel engines: Experiments and numerical simulations. SAE Tech Pap 2003. https://doi.org/10.4271/2003-01-1791.
[51] Zhu X, Andersson Ö. Performance of new and aged injectors with and without fuel additives in a light duty diesel engine. Transport Eng 2020;1:100007. https://doi.org/10.1016/j.treng.2020.100007.
[52] R. H. Barbour, R. Quigley, and A. Panesar, "Investigations into Fuel Additive Induced Power Gain in the CEC F-98-08 DW10B Injector Fouling Engine Test," *SAE Technical Papers*, vol. 2014-Octob, no. Idid, 2014, doi: 10.4271/2014-01-2721.
[53] Naseri H, Trickett K, Mitroglou N, Karathanassis I, Koukouvinis P, Gavaises M, et al. Turbulence and Cavitation Suppression by Quaternary Ammonium Salt Additives. Sci Rep 2018;8(1). https://doi.org/10.1038/s41598-018-25980-x.
[54] Karathanassis IK, Trickett K, Koukouvinis P, Wang J, Barbour R, Gavaises M. Illustrating the effect of viscoelastic additives on cavitation and turbulence with X-ray imaging. Sci Rep 2018;8(1):1–15. https://doi.org/10.1038/s41598-018-32996-w.
[55] I. K. Karathanassis et al., X-ray phase contrast and absorption imaging for the quantification of transient cavitation in high-speed nozzle flows, vol. 33, no. 3. 2021. doi: 10.1063/5.0038475.
[56] Naseri H, Koukouvinis P, Malgarinos I, Gavaises M. On viscoelastic cavitating flows: a numerical study. Phys Fluids 2018;30(3):pp. https://doi.org/10.1063/1.5011978.
[57] Heidari-Koochi M, Karathanassis IK, Koukouvinis P, Hwang J, Pickett LM, Spivey D, et al. Flow visualisation in real-size optical injectors of conventional, additised, and renewable gasoline blends. Energy Convers Manage 2022;252:115109.
[58] European Committee for Standardization, "EN 14214 Fatty acid methyl esters (FAME) Requirements and test methods," no. June, p. 10, 2014.
[59] Kolev NI. Thermodynamic and transport properties of diesel fuel. In: Kolev NI, editor. Multiphase Flow Dynamics 4. Berlin, Heidelberg: Springer Berlin Heidelberg; 2012. p. 293–327.
[60] SANDIA, "https://ecn.sandia.gov/," 2022.
[61] "https://ecn.sandia.gov/," 2022. https://ecn.sandia.gov/.
[62] Engine Combustion Network, "Spray D Nozzle Geometry," 2021. https://ecn.sandia.gov/diesel-spray-combustion/target-condition/spray-d-nozzle-geometry/.
[63] Naber JD, Siebers DL. Effects of gas density and vaporization on penetration and dispersion of diesel sprays. SAE Tech Papers 1996;no. 412. https://doi.org/10.4271/960034.
[64] Ptasinski PK, Boersma BJ, Nieuwstadt FTM, Hulsen MA, van den Brule HAA, Hunt JCR. Turbulent channel flow near maximum drag reduction: Simulations, experiments and mechanisms. J Fluid Mech 2003;490:251–91. https://doi.org/10.1017/S0022112003005305.
[65] Dubief Y, White CM, Terrapon VE, Shaqfeh ESG, Moin P, Lele SK. On the coherent drag-reducing and turbulence-enhancing behaviour of polymers in wall flows. J Fluid Mech 2004;514:271–80. https://doi.org/10.1017/S0022112004000291.
[66] Naseri H, Koukouvinis P, Karathanassis I, Gavaises M. Flow enhancement and cavitation suppression in nozzle flow by viscoelastic additives. In: Katz J, editor. Proceedings of the 10th International Symposium on Cavitation (CAV2018). ASME Press; 2019. p. 462–7. https://doi.org/10.1115/1.861851_ch88.